Polarization Properties of Vertical Cavity Surface Emitting Lasers

M. San Miguel

IMEDEA (Instituto Mediterráneo de Estudios Avanzados, CSIC-UIB) [1]
Campus Universitat Illes Balears
E-07071 Palma de Mallorca, Spain

1 Introduction

Vertical Cavity Surface Emitting Lasers (VCSELs) are expected to become some of the most popular laser diodes in the near future. Their general characteristics, performance, fabrication aspects and applications are reviewed in other chapters of this book (Blum, 1999; Ebeling, 1999). A peculiarity of these lasers, as compared to conventional edge emitting laser diodes, is that, due to their different geometry, the polarization of the laser light is not well stabilized. This becomes a problem for applications which require a well stabilized polarization and it has motivated the proposal of a number of methods to fix the polarization state of the emitted light. These methods include introducing polarization sensitive DBR mirrors (Ser et al., 1995), geometrical or stress-induced anisotropies (Mukaihara et al., 1993) or engineering of the semiconductor material or the growth process (Chavez-Pirson et al., 1993; Sun et al., 1975) to favor the gain of one of the two independent polarization directions. A different attitude is, instead of suppressing the vector degree of freedom associated with the polarization of light, to learn how to control and use it in possible applications based on the polarization state such as optical switching (Nishikawa et al., 1995; Kawaguchi and Kawakami, 1977), information processing or storage, etc. This requires the understanding of the basic physical mechanisms that control the polarization of laser light. Such understanding should make possible to follow the path indicated in the title of this school: "From quantum physics to smart devices". In these lectures I review, from a laser physics point of view, a macroscopic modeling of VCSELs which incorporates those basic mechanisms.

1.1 Phenomenology of Polarization Selection in VCSELs

Light emitted from VCSELs is typically linearly polarized, with the vector field randomly oriented in the plane transverse to the light emission direction or with a preferred orientation along one of two orthogonal crystal axis on that plane. Close to threshold the VCSEL generally emits in the fundamental transverse mode. With this transverse profile fixed the polarization direction can be stable as the injection current is increased (Koyama et al., 1991) or often a switch to the orthogonal polarization state occurs for some value of the injection current (Pan et al., 1993). A switch back to the polarization selected at threshold can also occur by further increasing the injection current (Choquette et al., 1994a). The switching processes still occur in a geometry which tends to equalize the gain of the two eigenpolarizations and when the cavity resonance is always detuned to the same side of the gain peak (Choquette et al., 1995a). The polarization switching often shows hysteresis (Kawaguchi et al., 1995), so that the switch occurs for different values of the injection current when this is increased and decreased. Polarization switching has also been observed when driving the laser with electrical pulses shorter than the thermal relaxation time, so that temperature effects do not come into play (Martín-Regalado et al., 1997c). Simultaneous emission in the two independent linearly polarized modes with different emission frequencies (Choquette et al., 1994b; Choquette

[1] Electronic address: http://www.imedea.uib.es/PhysDept

et al., 1995b) as well as in these two modes but with the same emission frequency (elliptically polarized light) (van Doorn et al., 1997) have been reported.

Transverse modes of higher order than the fundamental (Chang-Hasnain et al., 1991; Li et al., 1994) start lasing for values of the injection current that strongly depends on the dimensions of the stripe contact. It often occurs that after a polarization switching in the fundamental mode, further increase of the injection current leads to the appearance of a first order transverse mode (Choquette et al., 1994b; Ser et al., 1995). The polarization switching in the fundamental mode disappears if the diameter of the contact is reduced (Ser et al., 1995). It is commonly observed that the first order transverse mode starts lasing orthogonally polarized to the fundamental mode (Choquette et al., 1994b; Ser et al., 1995; Fiedler et al., 1996; Epler et al., 1996). There are however indications that this fact might be associated with a red shift of the gain relative to the cavity resonance, while for a strong blue-shift the first order transverse mode appears polarized parallel to the fundamental mode. In general the emergence of successive higher order modes is strongly correlated with changes of polarization (Epler et al., 1996).

Transverse modes of different order are separated in frequency 100-200 GHz, while transverse modes of the same order are separated in frequency by birefringence. This separation can vary from smaller than 1 GHz up to tens of GHz. Birefringence is believed to have two main origins. There is a main and systematic contribution due to the electro-optic effect during laser operation with a drive voltage (Hendriks et al., 1997) and a random contribution due to the elasto-optic effect (van Doorn et al., 1996b). The second contribution is due to residual strain in the fabrication process or in the electrical contacts. This effect can be used to change the value of the birefringence by locally burning holes in the device with a solid state laser (van Doorn et al., 1996a).

Thermal effects are another important aspect which influences polarization properties of VCSELs. Increasing the operating current produces selfheating of the device mostly due to the series resistance in the DBR mirrors. This leads to the reversible extinction of the output light. The reason for that is that the threshold current has a parabolic dependence with temperature. The resonant frequency selected by the short optical cavity red-shifts with temperature, but the gain profile shifts at a larger rate, so that eventually the resonance frequency is outside the range of frequencies for which there is positive gain. The minimum threshold current corresponds to alignment of the cavity resonance and the gain peak frequencies. The heating of the device also gives rise to thermal lensing that produces an effective index guiding effect.

1.2 What determines the polarization state of light?

This general question was posed and answered in rather general terms in the early days of laser physics (de Lang et al., 1971; van Haeringen, 1967; Lenstra, 1980; Stephan and May, 1998): The polarization state of light emitted by a laser depends on two main ingredients. The first one is the angular momentum of the quantum states involved in the emission or absorption optical transitions. Emission of a photon with right (left) circular polarization corresponds to an allowed optical transition in which the projection of the total angular momentum of the gain medium on the direction of light propagation changes by $+1$ (-1). This first ingredient of polarization selection reflects the nonlinear dynamics of the gain medium. The second ingredient is associated with the linear effects of the laser cavity. The anisotropies (birefringence, dichroism), geometry, detuning and waveguiding effects of the cavity lead to a preference for a particular polarization state of the laser light. These two ingredients can compete or be complementary, their relative importance depending on the type of laser.

Different atomic gas lasers emit linearly, circularly or elliptically polarized light, and such polarization states have been identified, for nearly isotropic laser cavities, with different atomic or molecular optical transitions. If the gain medium selects linearly polarized light, birefringence deter-

mines preferred directions for this linear polarization. Polarization switching between these preferred orientations can be then explained by phase-amplitude coupling due to the combined effect of birefringence and detuning: A switching between two orthogonally polarized modes with very similar gains is observed when changing the cavity length of a birefringent cavity (de Lang et al., 1971).

A natural question is which of those two ingredients of polarization selection matters in semiconductor lasers. For conventional edge emitting lasers, cavity effects associated with geometry are usually predominant: Light is polarized in the plane of the active region since the orthogonal direction has much larger cavity losses. However, the cylindrical symmetry of the VCSEL, together with the isotropy of the linear optical properties of III-V compounds grown on the [001] direction, make the nonlinear gain dynamics much more important. In addition, the linewidth enhancement factor of semiconductors (α-factor) gives the same type of amplitude-phase coupling than detuning in a gas laser, but its magnitude is considerably larger. By analogy with gas lasers, it is therefore expected that the combined effect of saturable dispersion associated with the α-factor and birefringence is also an important mechanism of polarization selection and in VCSELs.

In these lectures I discuss a model for polarization dynamics of VCSELs that takes into account those two ingredients. I mention here that two other simplified explanations of polarization selection in the fundamental transverse mode have also been proposed. Both disregard phase-amplitude couplings. They rely on the idea that the differences in gain of the two polarization modes stabilize one of the modes. A first explanation is based on the thermal effects discussed above: The two polarization modes have different gain because of their different frequency due to birefringence. As the injection current is increased the faster red-shift of the gain curve, as compared with the red-shift of the central resonant cavity frequency, leads to a change of sign in the gain difference between the two polarization modes, and thus to a polarization switching (Choquette et al., 1995b). Another mechanism invoked in weak index-guided VCSELs is the combined effect of birefringence and spatial-hole burning, which causes differences in the modal gain of the waveguide transverse modes with orthogonal polarization (Valle et al., 1996; Panajotov et al., 1998). In both explanations the differences in gain can be minute. These differences seem to be what determines which polarization is selected at threshold, but they do not seem enough to account for polarization switching. In any case they do not explain much of the phenomenology described above, so that additional physical mechanisms need to be considered. In particular, thermally induced switching does not account for hysteresis in the switching current and for the observed switchings at constant temperature.

1.3 Outline

In the next section the Spin Flip Model (SFM) for polarization dynamics is introduced (SanMiguel et al., 1995). In the context of this model the operation of a VCSEL in the fundamental transverse mode is discussed in section 3. Transverse effects in index and gain guided devices are discussed in section 4. Section 5 discusses polarization properties of optically pumped VCSELs. The differences between the susceptibility of a two-level type of model and a quantum well semiconductor are reviewed in the section 6. The consideration of a proper semiconductor susceptibility within the SFM model and its consequences on the dynamics of polarization selection are also outlined in the final section.

2 Spin Flip Model (SFM) for Polarization Dynamics

The geometry of the VCSEL is such that the laser vector electric field $\mathbf{E}$ lies in the plane transverse to the longitudinal direction z of light emission. Its linear components (E_x, E_y) and the circularly

(E_+, E_-) polarized components satisfy the relation

$$E_\pm = \frac{1}{\sqrt{2}}(E_x \pm iE_y). \tag{1}$$

A first important effect of the optical cavity is the selection of a longitudinal mode k_c with a resonant cavity frequency ν. Due to the the high mirror reflectivities of the VCSEL this produces a vectorial standing wave with a forward and backward propagating components. In a mean field approximation one can average out the longitudinal z dependence of these amplitudes and write the electric field as

$$\mathbf{E} = \mathbf{F}(x, y, t)e^{ik_c z - i\nu t} + c.c.. \tag{2}$$

One is interested in the equation satisfied by the slowly varying amplitude $\mathbf{F}(x, y, t)$ which can be understod as the amplitude of the selected longitudinal mode. From Maxwell's equations one identifies that the source of $\mathbf{F}$ is the slowly varying amplitude of the macroscopic material polarization $\mathbf{P}(x, y, t)$. The linear cavity effects amount to a linear cavity susceptibility matrix M. The basic equation for the field is then

$$\partial_t \mathbf{F} = \frac{ic^2}{2\nu n_e^2}\nabla_\perp^2 \mathbf{F} + \mathbf{P} - M\mathbf{F}. \tag{3}$$

The first term on the right hand side represents diffraction in the transverse plane (where n_e is the background index of refraction) and the other two terms are the two basic ingredients of polarization selection: material gain dynamics and effects of the optical cavity.

2.1 Cavity, Band Structure and Optical Transitions

The cavity susceptibility M can be written as

$$M = \kappa I - \Gamma, \tag{4}$$

where κ, which represents the cavity losses, is the inverse of the photon cavity lifetime. The matrix Γ represents the cavity anisotropies (van Haeringen, 1967). Generally speaking, the hermitian part of Γ is associated with anisotropic properties with respect to the moduli of the two complex components of the field (amplitude anisotropies or dichroism). The antihermitian part of Γ is associated with phase anisotropies (birefringence). The matrix Γ can be written in the linear or in the circularly polarized basis of the field. The diagonal elements of Γ in the linear basis are named linear anisotropies and the diagonal elements in the circular basis are the circular anisotropies. In the simplest case in which one can neglect circular anisotropies and when amplitude and phase anisotropies are along the same directions, Γ is written in the linear basis as

$$\Gamma = -(\gamma_a + i\gamma_p)\begin{pmatrix} 1 & 0 \\ 0 & -1 \end{pmatrix}. \tag{5}$$

γ_a is the amplitude anisotropy and gives different losses to the two linearly polarized components, while γ_p is the phase anisotropy which gives them a different frequency. Their separation in frequency is a measure of cavity birefringence.

The other basic ingredient in Eq.(3) is the material polarization $\mathbf{P}$ of the gain medium. The coupled set of equations for $\mathbf{F}$ and $\mathbf{P}$ receive the name of Maxwell-Bloch equations. Deriving an equation for $\mathbf{P}$ requires knowledge of the allowed optical dipole transitions underlying the electron-hole recombination process in the quantum well, and this, in turn, depends on the band structure of the semiconductor. The band structure of direct band gap III-V compounds, in the free carrier approximation, can be calculated perturbatively from the Bloch states found at zero transverse wave

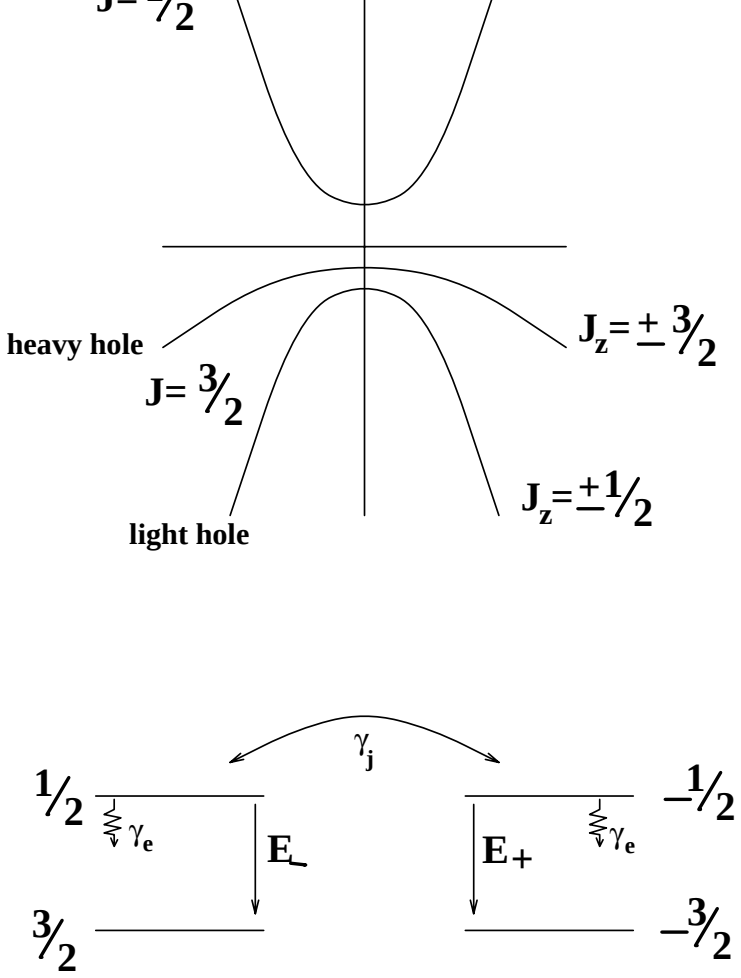

Figure 1: a) Schematic representation of the band structure of a quantum well. b) Lasing transitions associated with right (E_+) and left (E_-) circularly polarized emission. The two two-level systems are coupled by spin flip processes (γ_j).

number $k_\perp$(Chow et al., 1994). These states are important because they have a well defined quantum number for the angular momentum and fix the symmetries of the states. The conduction band state have the symmetry of an atomic s-state with zero orbital angular momentum, while the valance band states have the symmetry of an atomic p-state with orbital angular momentum $l = 1$. Due to spin orbit coupling the conduction band states have a total angular momentum $J = 1/2$, while the valence band states have $J = 3/2, 1/2$. The split-off valence band associated with the state $J = 1/2$ will be disregarded because of its lower energy. The quantum well confinement breaks the degeneracy of the $J = 3/2$ state leading to a HH (heavy hole) state ($J_z = \pm 3/2$) of higher energy than the LH (light hole) state ($J_z = \pm 1/2$). The band structure is calculated from these $k_\perp = 0$ states through a 4x4 matrix Luttinger Hamiltonian associated with the first energy level of the quantum well and the HH and LH states. The HH and LH bands emerge as indicated in Figure 1a, but there is band mixing, so that the two basis states of the HH band have a contribution of states with $J_z = \pm 1/2$. This general picture of band structure can be modified by effects of strain that will not be considered here.

In a first approximation one can neglect recombination processes from the conduction to the LH band which is at a lower energy than the HH band. For the transverse electric field of a VCSEL and for electronic states with $k_\perp = 0$, the allowed electric dipole transitions that result in electron-hole recombination are those in which $\Delta J_z = \pm 1$. Emission of right circularly polarized photons

corresponds to $\Delta J_z = -1$ and left circularly polarized photons to $\Delta J_z = +1$. For the electronic states at the band edge there are thus two allowed transitions between the conduction and heavy hole band: the transition from $J_z = -1/2$ to $J_z = -3/2$ associated with right circularly polarized light and the transition from $J_z = 1/2$ to $J_z = 3/2$ associated with left circularly polarized light. There picture that emerges is that of two two-level lasing transitions (two "channels" of light emission) with different circular polarizations as indicated in Figure 1b. Different processes that change the spin of the carriers with a spin flip rate γ_j couple these two two-level systems.

For electronic states with nonzero transverse wavenumber this picture is not so simple because of the band mixing discussed above. Still, the main contributions are well described by the simple scheme of Figure 1b. The main conceptual difference which occurs when considering band mixing effects is that they provide a nonlinear mechanism of coupling between the carrier densities associated with the two lasing transitions. For many purposes this just amounts to an effective value of the spin flip rate, so that no qualitative differences are found in the general properties of polarization selection and switching.

2.2 Maxwell-Bloch Equations, Susceptibility and Rate Equations

The dynamics of the radiation-matter interaction in the four-level model of Figure 1b follows from a standard density matrix calculation (Sargent et al., 1974). This analysis leads to a set of equations, which with Eq.(3), form the closed set of Maxwell-Bloch equations of the model (SanMiguel et al., 1995):

$$\partial_t F_\pm(x,y;t) = -\kappa(1+i\alpha)F_\pm + P_\pm + i\frac{c^2}{2\nu {n_e}^2}\nabla_\perp^2 F_\pm - (\gamma_a + i\gamma_p)F_\mp \quad (6)$$

$$\partial_t P_\pm(x,y;t) = -\gamma_\perp(1-i\alpha)P_\pm + \gamma_\perp a(D \pm d - D_0)F_\pm \quad (7)$$

$$\partial_t D(x,y;t) = C(x,y) - \gamma_e D + D_f\nabla_\perp^2 D - [(F_+P_+^* + F_-P_-^*) + c.c.] \quad (8)$$

$$\partial_t d(x,y;t) = -\gamma_s d + D_f\nabla_\perp^2 d - [(F_+P_+^* - F_-P_-^*) + c.c.]. \quad (9)$$

These equations are written for the two circularly polarized components of $\mathbf{F}$ and $\mathbf{P}$ which correspond naturally to each of the two coupled two-level systems of Figure 1b. Eq.(6) is just Eq.(3) where the form of Γ in Eq.(5) has been used and where the equations are written with a change of reference frequency such that the laser emission frequency is close to zero at threshold. This introduces in Eq.(6) the normalized detuning between the resonant cavity frequency ν and the bandgap frequency ω_g (frequency difference between the upper and lower levels of Figure 1b):

$$\alpha = \frac{\nu - \omega_g}{\gamma_\perp} \quad (10)$$

where $\gamma_\perp$ is the decay rate of the material polarization. Each component of the material polarization $P_\pm$ is directly coupled to the carrier density $D_\pm$ of the corresponding two-level system with a differential gain parameter a. The variable $D = D_+ + D_-$ represents the total carrier density referred to its transparency value D_0, while $d = D_+ - D_-$ represents the difference between the two carrier populations associated with emission of E_+ and E_-. The two channels of emission are pumped with the same injection current $C(x,y)$. In these equations one has further introduced in a phenomenological way carrier diffusion with diffusion coefficient D_f, a decay rate γ_e for electron-hole recombination and a decay rate $\gamma_s = \gamma_e + 2\gamma_j$ which takes into account the spin relaxation processes that mix the carrier populations with opposite values of J_z. A detailed derivation of Eqs.(6)-(9) can be found elesewhere (SanMiguel et al., 1995; Martin-Regalado, 1997). Note that this type of modeling does not include thermal effects and presumes a symmetry in the transverse plane that only exists for ordinary VCSELs grown on the [001] crystallographic direction.

Eqs.(6)-(9) can be simplified in the spirit of the ordinary rate equations of a semiconductor laser (Agrawal and Dutta, 1986) when restricting them to situations in which a single transverse mode is relevant. In this case one looks for equations for the amplitude of this mode, which fixes a transverse profile, and diffraction and carrier diffusion are eliminated from the description. In addition one invokes large differences in the time scales of relaxation to eliminate the material polarization: The spin mixing described by γ_s typically occurs on larger time scales than photon decay, where $\kappa^{-1} \approx 1$ ps. The fastest time scale included in Eqs.(6)-(9) is the material polarization decay rate $\gamma_\perp^{-1}$ which is on the order of tens of femtoseconds, while the slowest decay is given by the carrier decay rate $\gamma_e^{-1} \approx 1$ ns. Therefore

$$\gamma_\perp >> \gamma_e, \gamma_s, \kappa \tag{11}$$

so that in time scales relevant for VCSEL operation $\mathbf{P}$ follows the dynamics of the other variables and it can be adiabatically eliminated. Note however, that d typically evolves in a dynamical scale intermediate between D and $F_\pm$ and, within this model, it plays a crucial role in the nonlinear dynamical properties of the VCSEL. The elimination of $\mathbf{P}$ defines, through Eq.(7), a susceptibility matrix χ,

$$\mathbf{P} = ia\chi\mathbf{F}, \tag{12}$$

where the form of χ in the circular and linear polarization basis is

$$\chi_\pm = \delta \begin{pmatrix} D + d - D_0 & 0 \\ 0 & D - d - D_0 \end{pmatrix}, \quad \chi_{x,y} = \delta \begin{pmatrix} D - D_0 & id \\ -id & D - D_0 \end{pmatrix}. \tag{13}$$

This form of χ indicates that the difference in carrier populations associated with the emission of E_+ and E_-, given by the variable d, gives a different susceptibility for the two circularly polarized components and breaks the rotational symmetry in the x, y plane. The prefactor δ has the typical form of a two-level susceptibility

$$i\delta = \frac{1 + i\alpha}{1 + \alpha^2} \tag{14}$$

with an imaginary part associated with gain and a real part which gives dispersion (index of refraction). The conventional α-factor (Henry, 1982; Osinski and Buus, 1987) of semiconductor lasers defined by

$$\alpha = -\frac{Re(\partial_D \chi)}{Im(\partial_D \chi)} \tag{15}$$

appears here as the normalized detuning (10).

Upon elimination of the material polarization replacing (12) in Eqs.(6),(8),(9) and an appropriate choice of units so that

$$E_\pm \sim F_\pm, \;\; N \sim (D - D_0), \;\; n \sim d$$

one finds

$$\frac{dE_\pm}{dt} = \kappa(1 + i\alpha)(N \pm n - 1)E_\pm - (\gamma_a + i\gamma_p)E_\mp \tag{16}$$

$$\frac{dN}{dt} = -\gamma_e(N - \mu) - \gamma_e(N + n)|E_+|^2 - \gamma_e(N - n)|E_-|^2 \tag{17}$$

$$\frac{dn}{dt} = -\gamma_s n - \gamma_e(N + n)|E_+|^2 + \gamma_e(N - n)|E_-|^2, \tag{18}$$

where μ is the spatially integrated injection current normalized to threshold.

As compared with Eqs.(6)-(9), these equations do not contain a frequency dependent gain and dispersion, whose values have been fixed at the operating frequency of the laser. As a consequence, the two polarization modes, splitted in frequency by birefringence, are given the same material gain. However, small differences in gain associated with birefringence can be taken into account through the amplitude anisotropy parameter γ_a. While in (6)-(9) this parameter only models intrinsic cavity anisotropies, it can also be used here to account for material gain differences. Eventually it can be made to depend on injection current or temperature.

2.3 Physical Processes: α-factor and Spin Flip Rate

In addition of nonlinear gain mechanisms, the model given either by the set of Eqs.(6)-(9) or the set (16)-(18) includes three fundamental physical processes, which will be shown to control the polarization state to a large extent: Phase-amplitude coupling introduced through the α-parameter, birefringence (γ_p) and spin mixing (γ_s). In the limit of very fast spin relaxation so that $n = 0$, and disregarding phase dynamics ($\alpha = 0$, $\gamma_p = 0$), (16)-(18) reduce to the conventional rate equation description of a semicondutor laser in terms of photon and carrier numbers (Agrawal and Dutta, 1986).

In the study of the semiconductor laser the α-parameter accounts for three main related effects: phase-amplitude coupling which introduces saturable dispersion, broadening of the linewidth ("linewidth enhancement factor") and carrier antiguiding ("antiguiding factor"). We are not here concerned with the linewidth of the laser (see for example (Ebeling, 1999)). Phase-amplitude coupling is included through the consideration of equations for the complex field amplitudes. It is important to note that, at the level of description of (16)-(18), and from a formal point of view, the sign of α is not important since the equivalent equations for the complex conjugate fields have the opposite sign of α. For the same reason the absolute sign of γ_p is not important, but only its sign relative to the one of α. Of course, the absolute direction of frequency chirp depends on the choice of the sign of α together with the frequency reference frame (Eq.2). The guiding or antiguiding effect requires the consideration of transverse effects, and its sense is determined by the relative sign of α and the diffraction term in (6)-(9). This point, together with a critical analysis of the use of two-level type susceptibilities for a semiconductor laser will be further discussed in section 6.

The spin flip rate γ_s has to be considered in this model as an effective parameter describing a variety of microscopic processes. From the point of view of laser physics it is also a mechanism of gain saturation. Spin relaxation processes in semiconductor materials (Meier and Zachachrenya, 1984) have been studied through polarization and time resolved photoluminescence experiments (Damen et al., 1991; Bar-Ad and Bar-Joseph, 1992; Oestreich et al., 1996), through the polarization dependence of photoluminescence light with the strength of a transverse magnetic field under continuous optical excitation (Hanle effect) (Fishman and Lampel, 1977; Snelling et al., 1991) and also through time resolved magneto-optical techniques (Kikkawa et al., 1997; Kikkawa and Awschalom, 1998). Important differences are found in bulk and quantum well materials and different mechanisms exist for spin relaxation of electrons, holes and excitons that in addition are known to be temperature and doping dependent. In a VCSEL in operating conditions there is a dense plasma of electron and holes with no significant exciton contribution. Since holes in a quantum well are known to relax much faster than electrons, the important spin relaxation processes are those of the electrons at roomtemperature. Experimental results for quantum well materials give a characteristic time of electron spin relaxation which typically ranges from about 10 ps at room temperature to 200 ps at low temperature (Sham, 1993; Tackeuchi et al., 1996). Recent results on undoped and n-doped quantum wells indicate that spin dynamics at room temperature are dominated by electrons and confirm an electron spin relaxation time of tens of picoseconds (Britton et al., 1998; Miller, 1999). However, electron spin lifetimes of nanoseconds have been measured in moderately n-doped II-VI semiconduc-

tor quantum wells at room temperature (Kikkawa et al., 1997). The spin lifetime is found to be a nonmonotonic function of carrier density, and for a lower n-doping level of bulk Ga-As semiconductor materials, lifetimes larger than 100 ns have been observed at a temperature of 5 K (Kikkawa and Awschalom, 1998). These lifetimes are far longer than the electron-hole relaxation time and in these cases the spin lifetime becomes the slow time scale of the system. Three main mechanisms have been identified for electron spin relaxation (Fishman and Lampel, 1977; Sham, 1993): Elliot-Yafet (due to spin-orbit interaction), Bir-Aranov-Pikus (exchange interaction between electron and holes) and Dyakonov-Perel. The latter arises from the lack of inversion symmetry in III-V compounds giving a spin sublevel splitting which can be regarded as an effective magnetic field. While there are indications that the Bir-Aranov-Pikus mechanism dominates at low temperatures when the holes density is important (Sham, 1993), the Dyakonov-Perel mechanism consistently explains the data for undoped and n-doped samples at room temperature (Tackeuchi et al., 1996; Kikkawa et al., 1997; Britton et al., 1998).

Very little is known about the relative importance of the different mechanisms of spin relaxation and the value of the electron spin relaxation time under the high-density, room temperature conditions of a VCSEL above the lasing threshold. Some proposals and experiments, however, have been made to determine γ_s on the basis of the SFM model introduced above. One is based on measuring the effect of a longitudinal magnetic field on the ellipticity of the emitted light due to the Zeeman splitting of the magnetic sublevels (Serrat et al., 1996; van Doorn et al., 1997). Another one is based on the fitting of results for the value of the injection current at which a polarization switching occurs under conditions of constant temperature (Martín-Regalado et al., 1997c; Martin-Regalado, 1997). Other measuraments (van Exter et al., 1998a) are based on the fluctuations of the ellipticity and the polarization direction as well as on properties of the optical spectrum (van der Lem and Lenstra, 1997; van Exter et al., 1998b). A final proposal is based on the analog of the Hanle effect for an optically pumped VCSEL (Gahl et al., 1998). These studies give an estimate of the characteristic time of spin relaxation in the range of 1-15 ps. Given their character of indirect measurements, the actual value of the electron spin relaxation time and of the effective parameter γ_s determined from them is rather uncertain. However, it will be seen that polarization selection and switching is very sensitive to its precise value.

3 Fundamental Transverse Mode Operation

The basic model given by Eqs.(16)-(18) describes a VCSEL operating in the fundamental transverse mode with two polarization modes with different frequencies. The predictions of this model concerning polarization selection and polarization switching are summarized in this section (Martín-Regalado et al., 1997d).

3.1 Basic Polarization States

The set of Eqs.(16)-(18) admit a number of solutions which can be generally written as

$$E_\pm = Q_\pm e^{i(\omega_\pm t \pm \psi) + i\theta} \ , \quad N = N_0 \ , \quad n = n_0 \ , \tag{19}$$

where θ is the arbitrary laser phase. Solutions with a well defined polarization are those with a single frequency ($\omega_+ = \omega_-$). Circularly polarized solutions are those in which either $Q_+ = 0$ or $Q_- = 0$. Linearly polarized solutions are those with $Q_+ = Q_-$. For these solutions the angle ψ gives the orientation of the linearly polarized light in the x, y plane. Ellipticaly polarized solutions are those in which the two real amplitudes $Q_\pm$ are nonzero and different. The ellipticity of these solutions is given by $(Q_+ - Q_-)/(Q_+ + Q_-)$

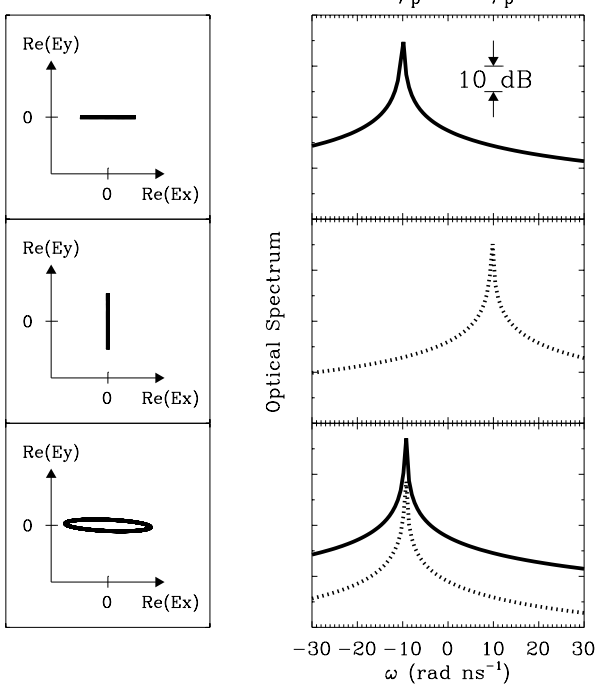

Figure 2: Basic polarization states obtained for $\gamma_a = 0$. The optical spectra of the complex field amplitudes E_x (continuous line)and E_y (dashed line) is shown. The frequency splitting between the two linearly polarized modes is $2\gamma_p$. They frequency lock in the elliptically polarized state, but have different power strengths.

Circularly polarized states are never found to be stable solutions of (16)-(18). For a perfectly isotropic VCSEL ($\gamma_a = \gamma_p = 0$) linearly polarized states exist, but with an arbitrary orientation ψ. Birefringence alone (γ_p) is able to fix the direction of polarization selecting two preferred values of ψ which can be identified with the $\hat{x}$– and $\hat{y}$–linearly polarized states. Additionally, one finds elliptically polarized states in which the the $\hat{x}$– and $\hat{y}$– linearly polarized modes are frequency locked (Figure 2)

In general the $\hat{x}$–polarized solution is given by

$$Q_{\pm}^2 = \frac{1}{2}\frac{\mu - N_0}{N_0} , \qquad \psi = 0 , \tag{20}$$

$$\omega_{\pm} = \omega_x = -\gamma_p + \gamma_a \alpha , \tag{21}$$

$$N_0 = 1 + \frac{\gamma_a}{\kappa} , \qquad n_0 = 0 , \tag{22}$$

while the $\hat{y}$–polarized solution is

$$Q_{\pm}^2 = \frac{1}{2}\frac{\mu - N_0}{N_0} , \qquad \psi = \frac{\pi}{2} , \tag{23}$$

$$\omega_{\pm} = \omega_y = \gamma_p - \gamma_a \alpha , \tag{24}$$

$$N_0 = 1 - \frac{\gamma_a}{\kappa} , \qquad n_0 = 0 . \tag{25}$$

These two states have different amplitudes and different threshold values $\mu_{th} = N_0$ due to the amplitude anisotropy γ_a. This anisotropy also causes that the frequency difference $\omega_x - \omega_y$ does not coincide with the birefringence induced splitting $2\gamma_p$. Note that which of the two linearly polarized modesis the high frequency mode depends on the sign of γ_p as well as on the choice of reference frame (Eq.2).

In addition of these basic states with a well defined polarization, it is also possible to find states in which the two independent components of the polarization have different amplitudes and a different frequency (or several frequencies). Those dynamical states describe polarization mode partition which would be experimentally observed as a finite time averaging of these states.

3.2 Stability analysis

A linear stability analysis of the basic polarization states introduced above describes the growth or decay of small fluctuations around these states. This analysis identifies the relevant parameters and mechanisms which control polarization selection and switching. The eigenvalues found in such a linear analysis determine the stability boundaries of the different polarization states. They also determine the response to spontaneous emission fluctuations, and therefore the properties of the optical spectrum (van der Lem and Lenstra, 1997; van Exter et al., 1998b). The main qualitative conclusions of such analysis for the linearly polarized states are the following (Martín-Regalado et al., 1997d):

- The linear problem is always separable in two independent problems. The first problem refers to the fluctuations of the total laser intensity $I = |E_+|^2 + |E_-|^2$ and the total carrier number N, and it is independent of cavity anisotropies (γ_a and γ_p), as well as of the spin relaxation rate γ_s. The analysis of this first problem just reproduces the well known relaxation oscillations of a semiconductor laser. It is equivalent to what follows from ordinary rate equations for the laser intensity and the total carrier density (Ebeling, 1999). The second problem contains all the properties of the polarization dynamics. It describes coupled fluctuations of $E_+ - E_-$ with the difference in carrier populations with different spin number (n). Equivalently, it describes coupled fluctuations of the direction of polarization ψ, ellipticity and n.

- Inspection of the characteristic equation that determines the stability of linearly polarized states reveals the importance of different parameters. For the perfectly symmetric laser ($\gamma_a = \gamma_p = 0$) there is a vanishing eigenvalue associated with the arbitrary orientation of the linearly polarized state. For a nonisotropic laser there are domains of parameters in which either only one of the linearly polarized states is stable, or the two are linearly stable (bistability) or none is stable (see Figures 3 and 4). If $\gamma_p = 0$ only one of the two linearly polarized solutions is stable. When $\alpha = 0$, the domain of bistability is the only one that survives. This is strictly so for $\gamma_a = 0$, but still true for reasonably small γ_a except for extremely large or small birefringence. Therefore, for $\alpha = 0$ and typicalvalues of the other parameteres, whatever state is selected at threshold (due to a lower threshold because of amplitude anisotropies), it will always remain stable. The change in the relative stability of the two linearly polarized modes is thus due to the combined effect of birefringence and saturable dispersion. Likewise, in the limit of infinitely fast spin relaxation ($\gamma_s^{-1} = 0$) there is again only bistability. A finite spin relaxation time is thus a necessary condition for changes of stability and polarization switching.

- In the domain of parameters in which a linearly polarized state is stable its optical spectrum shows two qualitatively different regimes. These regimes are better understood for small amplitude anisotropies ($\gamma_a \sim 0$): For the symmetric laser ($\gamma_p = 0$) there is a regime of fast spin relaxation with exponential relaxation of fluctuations and a regime of slow spin relaxation in which one finds damped "polarization relaxation oscillations" (SanMiguel et al., 1995). In these oscillations the ellipticity and n oscillate at a frequency of the order of the laser relaxation oscillations. The two regimes are separated by a critical value of the spin flip rate γ_s of the order of the frequency of the relaxation oscillations. For non vanishing birefringence, this second regime is continued into one in which the "polarization relaxation oscillations" persist far from

threshold, while fluctuations of the direction of polarization ψ (fixed by birefringence) relax exponentially. However, close to threshold and for fast spin relaxation, a new regime appears in which n relaxes exponentially with a time constant γ_s^{-1} while damped coupled oscillations of the ellipticity and the polarization orientation ψ emerge. These oscillations occur at a frequency which grows linearly with the distance to threshold. This frequency is thus different from the relaxation oscillation frequency which grows with the square root of the distance to threshold. It seems that many VCSELs operate in this last regime, and optical spectra showing these oscillations have been recently measured (van Exter et al., 1998a). Note however that relatively small variations in injection current and spin flip rate lead from one to the other of the two regimes just described.

3.3 Polarization Switching

Polarization switching occurs when one of the two linearly polarized states looses stability. The switching point is obtained from the analysis discussed above. For a fixed value of the α-parameter this is studied in terms of two control parameters commonly measured in experiments of polarization switching, the injection current μ normalized to the threshold current, and birefringence measured by γ_p. Typical polarized light-current measurements correspond to vertical scannings in (μ, γ_p) diagrams since birefringence is a fixed characteristic of a given VCSEL, which is nearly independent of the injected current. Stability diagrams are summarized in Figure 3 and Figure 4. These figures correspond to two general situations in which the relative gain-to-loss ratio between the modes, given by γ_a, is different. In each case a different polarization state is selected at threshold. In both cases elliptically polarized states are only stable in a narrow range of parameters along the curve that determines the stability of the $\hat{x}$-polarized solution and in the side of low birefringence.

Figure 3 shows the stability diagram for VCSELs where the gain difference favors the $\hat{y}$-polarized mode at threshold ($\gamma_a > 0$) so that the threshold for the $\hat{x}$-polarized mode is higher than for the $\hat{y}$-polarized mode ($\mu_{th}^x > \mu_{th}^y$). The $\hat{y}$-polarized mode is stable to the left and below the dashed line. The $\hat{x}$-polarized mode is stable to the right and above the solid line. Stable $\hat{y}$-polarized emission occurs close to threshold for any value of the birefringence. For low birefringence VCSELs such that $\gamma_p < \gamma_s/(2\alpha)$, the $\hat{y}$-polarized mode selected at threshold remains stable as the injection current is increased. However, if $\gamma_p > \gamma_s/(2\alpha)$, an abrupt $\hat{y} \to \hat{x}$ switching occurs as the dashed line is crossed when increasing the injected current. The switching occurs by destabilization of the mode with the higher gain-to-loss ratio in favor of the weaker mode. In addition, the switching current μ_{sw} linearly depends on the amplitude anisotropy γ_a,

$$\frac{\mu_{sw}}{\mu_{th}^y} = 1 + \frac{2(\gamma_s^2 + 4\gamma_p^2)}{\kappa(2\alpha\gamma_p - \gamma_s)} \frac{\gamma_a}{\gamma_e} \,. \tag{26}$$

Such a dependence is consistent with experimental results in gain-guided VCSELs operated at constant temperature of the active medium (Martín-Regalado et al., 1997c). Note also that when decreasing the injection current the reverse switching $\hat{x} \to \hat{y}$ would occur when crossing the continuous line, so that hysteresis in the switching current is predicted.

For gain differences favoring $\hat{x}$-polarization $\gamma_a < 0$, so that $\mu_{th}^x < \mu_{th}^y$. In this case the $\hat{x}$- polarized mode is stable below the solid line, while $\hat{y}$-polarization is stable to the left and above the dashed curve (see Figure 4). Stable $\hat{x}$-polarized emission is expected close above threshold for any birefringence value. For VCSELs in which $\gamma_p < \gamma_s/(2\alpha)$, $\hat{x} \to \hat{y}$ polarization switching occurs when the injection current is increased so that the solid line is crossed. The switching is again from the mode of higher gain to the one of lower gain and higher threshold. The switching current is given by

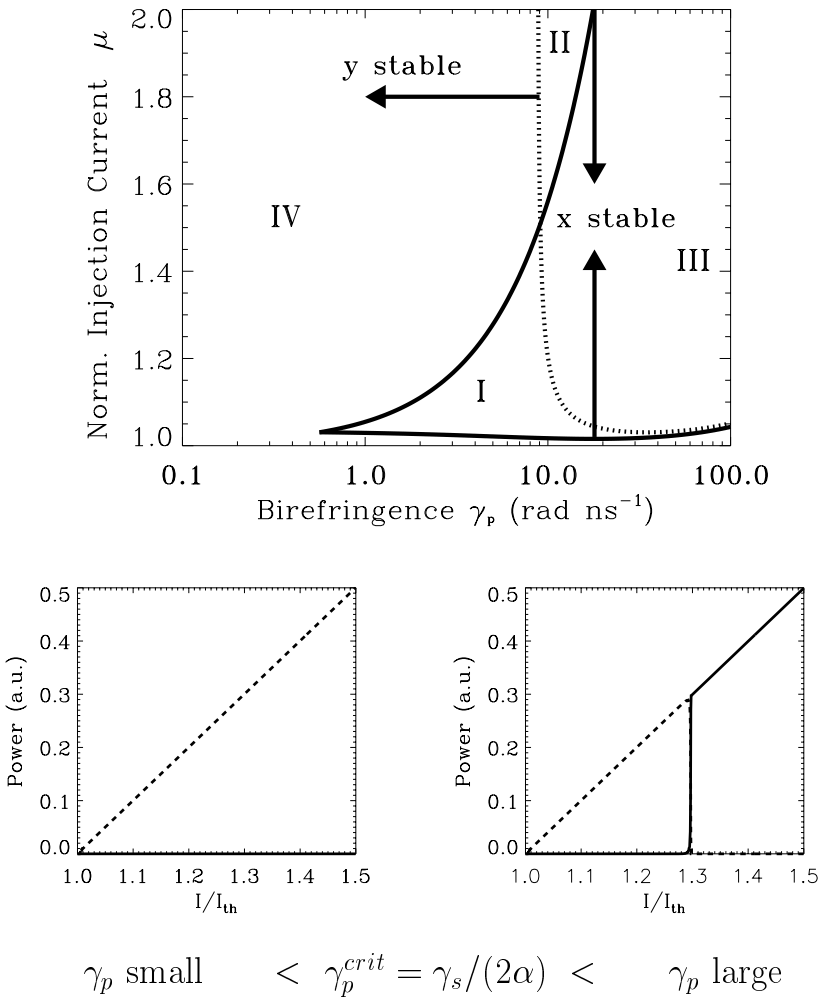

Figure 3: Stability diagram and polarization switching for positive amplitude anisotropy. In region I the two linearly polarized solutions are stable (bistability region) and in region II none of them is stable. In region III $\hat{x}$-polarized solution is stable and in region IV the $\hat{y}$-polarized solution is stable. Polarization stability for small birefringence and polarization switching for high birefringence are shown in the bottom figures, where solid (dashed) line corresponds to the output power of the $\hat{x}$ ($\hat{y}$)-polarized mode.

$$\frac{\mu_{sw}}{\mu_{th}^{x}} = 1 + \frac{(\gamma_p^2 + \gamma_a^2)}{\kappa(\gamma_a + \alpha\gamma_p) - \gamma_p^2}\frac{\gamma_s}{\gamma_e} \, . \tag{27}$$

This switching is not abrupt. Rather it occurs through one of two frequency-degenerate stable elliptically polarized states. Consequently, elliptically polarized light appears as intermediate states reached in the destabilization of the linearly polarized solution as the current is increased. Hysteresis in the switching current, is also predicted here.

The general discussion in section 3.2 makes clear the role of the parameters α, γ_p and γ_s in determining the stability properties of the different polarization states. According to this discussion and to the expressions for the switching currents (26)-(27) one concludes that the basic mechanisms that produce polarization switching in the VCSEL model analyzed here are i) coupling through spin flip processes (γ_s) of the two carrier populations with different spin number, and ii) the combined effect of birefringence (which couples the two circularly polarized components of the field) and phase-amplitude coupling (with associated saturable dispersion) produced by the α-factor.

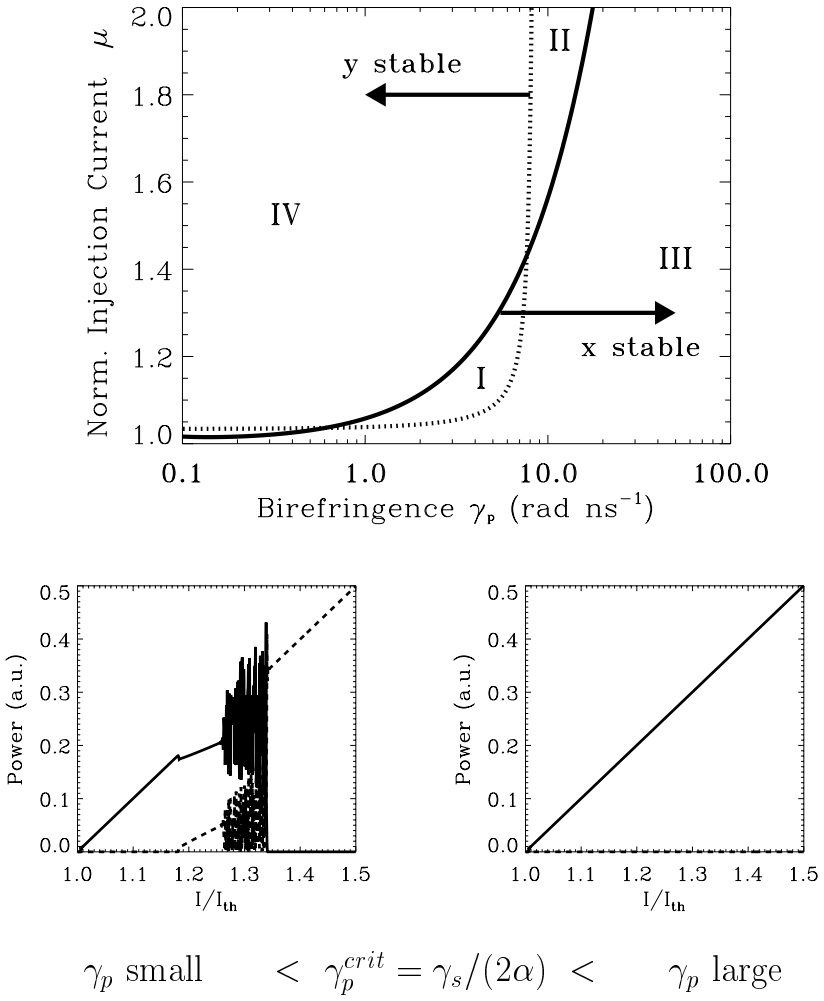

Figure 4: Stability diagram and polarization switching for negative amplitude anisotropy. Same meaning of regions I-IV than in Figure 3. Polarization switching through dynamical states for small birefringence and polarization stability for high birefringence are shown in the bottom figures, where solid (dashed) line corresponds to the output power of the $\hat{x}$ ($\hat{y}$)-polarized mode.

It is finally important to note that Figures 3 and 4 are for $\alpha > 0$ and $\gamma_p > 0$. Changing the sign of γ_p changes the low frequency mode into the high frequency mode. Changing the sign of α means, in the context of the derivation given here of Eqs.(16)-(18), changing the sign of the detuning (10). If γ_a is interpreted as arising from a difference in material gain due to birefringence, γ_a also changes sign when the sign of the detuning changes. If the sign of α and γ_a are changed, what happens is that the $\hat{x}$-polarized mode becomes stable in the (μ, γ_p) domain in which the $\hat{y}$-polarized mode was stable and viceversa. Therefore, changing the sign of α leaves unchanged the existence of a polarization switching and its nature (abrupt for large birefringence and through intermediate dynamical states for low birefringence), but the direction in frequency (high $\rightarrow$ low or low $\rightarrow$ high) is reversed.

3.4 Optical injection

Polarization switching can also be produced by optical injection (Kawaguchi and Kawakami, 1977) for a fixed value of the electrical injected current: Injecting into the laser an optical signal whose polarization is orthogonal to that emitted by the laser can produce a polarization switching. Two different situations have to be considered, switching by an optical pulse (Kawaguchi et al., 1995)

or switching by continuous optical pump (Pan et al., 1993). In the first case polarization switching occurs for pulses above a certain injected energy which depends on the detuning between the injected signal and VCSEL frequencies. The fact that the VCSEL remains in the new polarization state after the switching indicates that it is operating in a bistable domain (region I of Figures 3 and 4). Switching under continuous optical injection is needed when the VCSEL operates in a domain in which only one of the polarization states is stable, such as in regions III and IV of Figures 3 and 4. In this case the laser goes back to the initial state soon after the injected signal is removed. The switching on and off occur for different values of the injected power as this is increased and decreased. These values depend on the frequency of the injected signal, being the switching power minimum when the injected frequency locks to the frequency of the laser after the switching. This resonant frequency also separates a region of gradual transition from one of abrupt switching.

Both types of optical switching can be well described by the general model (16)-(18) supplemented by an injected field (Martín-Regalado et al., 1997d). In particular, the experiments of (Pan et al., 1993) are seen to correspond to switching by injection of a $\hat{y}$ polarized field in a laser operating in region III of Figure 3. A quantitative comparison requires knowledge of the VCSEL parameters introduced in (16)- (18). Besides other general parameters, birefringence is determined by the frequency splitting between the two linearly polarized states and the amplitude anisotropy parameter γ_a is fixed by the value of the switching current (26) when no optical field is injected.

3.5 Longitudinal Magnetic Field

Applying a magnetic field in the direction of laser light emission gives and additional way to probe the mechanisms of polarization selection in a VCSEL. It also opens the possibility of obtaining fast polarization modulation of the laser output (Serrat et al., 1996; van Doorn et al., 1997; van der Lem et al., 1998). Within the scheme of Figure 1b, the main effect of the magnetic field is a Zeeman splitting of the magnetic sublevels that results in different frequencies $\omega_\pm$ (different energy differences) for the emission of right and left circularly polarized light. Such frequency difference for E_+ and E_- can be modeled by including a circular phase anisotropy in the matrix Γ in (3)-(4). This amounts to add a term $\pm i\gamma_z E_\pm$ to the right hand side of (16), where γ_z is a measure of the strength of the magnetic field.

For weak magnetic fields linearly polarized emission becomes elliptically polarized and switching occurs between ellipticaly polarized states with different orientations of the main axis of the polarization ellipse. The dependence of ellipticity on magnetic field and injection current, as obtained experimentally, gives a useful way of determining different VCSEL parameters such as the spin flip rate. For moderate magnetic fields the optical spectra shows several frequencies and the polarization becomes modulated in both ellipticity and orientation. For strong magnetic fields ($\gamma_z >> \gamma_p, \gamma_a$), which can be of the order of 1 Tesla, the output emission is almost linearly polarized but with a direction of polarization that rotates in time. This implies that the $\hat{x}$ and $\hat{y}$ polarized output power oscillate in antiphase with a frequency $2\gamma_z$ which is predicted to be of a few GHz.

4 Transverse Effects and Polarization

Operation of a VCSEL on a single transverse mode has been considered in the previous section. In that discussion transverse spatial effects such as carrier diffusion, light diffraction and spatial hole burning have been neglected. These effects have some importance in the fundamental transverse mode operation, but they become more important when considering excitation of higher order transverse modes. In this case, due to the large separation in frequency of the different transverse modes, consideration of a frequency dependent gain and refractive index become also essential.

Transverse effects are very much dependent on the form of transverse light confinement. For index guided devices, mode profiles are well defined and the strategy is then to write equations for the amplitudes of these modes, much in the spirit of Eqs.(16)-(18). However, for gain guided devices there is no proper waveguide and modes are not well defined. Therefore, the complete set of partial differential Eqs.(6)-(9) must be considered. Proper boundary conditions are determined by the transverse profile of the injected current.

4.1 Index Guided Devices

For cylindrically symmetric weak index-guided devices, birefringence is taken into account by assuming that the core refractive index in the $\hat{y}$ direction is smaller than in the $\hat{x}$ direction, while the cladding refractive index is the same in both directions. The appropriate built-in transverse modes are then the LP_{mn} modes (Valle et al., 1995). Considering a VCSEL with a radially symmetric cavity that can operate in the fundamental and in the first–order transverse modes, the optical field can be written as

$$\mathbf{F}(r;t) = \left[\left(E_{0,x}(t)\psi_{0,x}(r) + E_{1,x}(t)\psi_{1,x}(r)\right)\hat{\mathbf{x}} + \left(E_{0,y}(t)\psi_{0,y}(r) + E_{1,y}(t)\psi_{1,y}(r)\right)\hat{\mathbf{y}}\right] + cc, \tag{28}$$

where r is the radial coordinate and subscripts (0,1) denote the LP_{01} and the LP_{11} modes, respectively, obtained by solving the Helmholtz equation (Valle et al., 1996). $\psi_{0,i}$ and $\psi_{1,i}$ are the modal profiles of the LP_{01} and LP_{11} modes and $E_{0,i}$ and $E_{1,i}$ are the modal amplitudes of these modes. The subindex $i = x, y$ stands for the linear polarization state of the given mode. The theoretical description proceeds by projecting Eqs.(6)-(9) into equations for the amplitudes $E_{0,i}$ and $E_{1,i}$ (Martín-Regalado et al., 1997b; Valle et al., 1998). The equations obtained in this way include modal gain coefficients $g_{j,i}(t)$ $(j = 0, 1;\ i = x, y)$, defined as

$$g_{j,i} = \frac{\int_0^\infty N(r;t)\psi_{j,i}^2(r)rdr}{\int_0^\infty \psi_{j,i}^2(r)rdr}, \tag{29}$$

as well as polarization cross-gain coefficients associated with the carrier population variable $n(r,t)$.

For the fundamental transverse mode operation, differences in gain between the $\hat{x}$ and $\hat{y}$ polarized modes, as obtained from (29), are due to the combined effect of birefringence and spatial-hole burning. These differences become smaller the larger is the step of refraction index, since this implies that the two polarization modes become better confined and have a more similar mode profile. Such differences in the modal gain have been invoked as a mechanism of polarization selection (Valle et al., 1996; Panajotov et al., 1998). The question is how this mechanism competes with the polarization effects attributed to spin dynamics and to the α-factor discussed in the previous section. It turns out (Martín-Regalado et al., 1997b) that for typical VCSEL parameters these gain differences are very small, but still effective to determine the polarization mode selected at threshold. The parameter γ_a used in the discussion of section 3 can be understood as a way of modeling these gain differences. However, as the injection current is increased, this selection mechanism is easily overcome by the mechanisms discussed in section 3. 2 and polarization switching to the polarization mode of lower gain occurs. Hole burning only causes a small quantitative impact in the location of the switching point, but it does not alter its nature.

Considering the fundamental and first order transverse mode a variety of phenomena occur for different parameter values (Valle et al., 1998), but unless polarization switching mechanisms are eliminated, the first order transverse mode appears typically orthogonally polarized to the fundamental transverse mode.

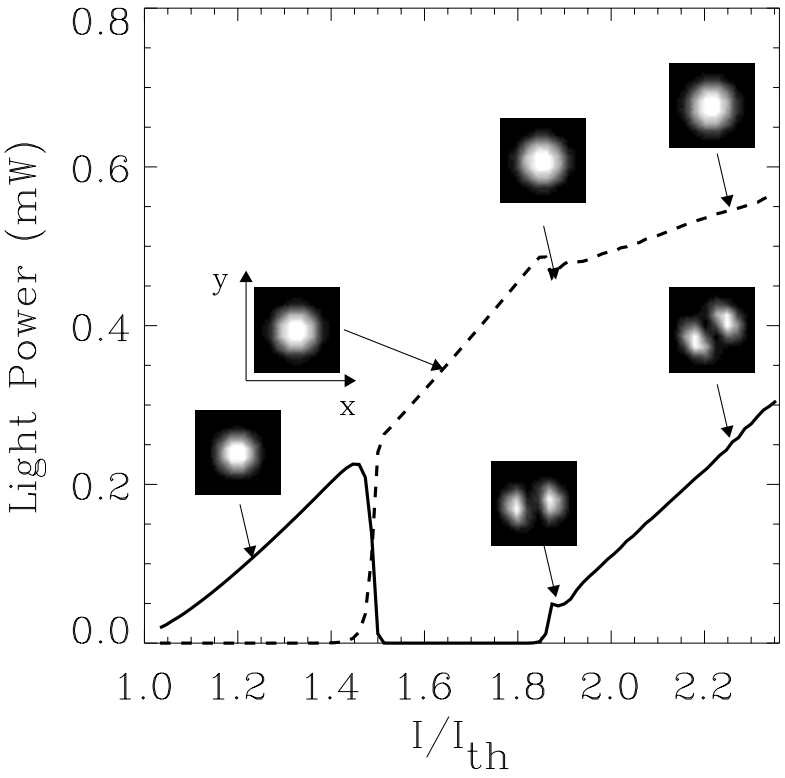

Figure 5: L-I characteristic for the linearly $\hat{x}$ (solid) and $\hat{y}$ (dashed) polarizations. The near field transverse profile of each polarization is shown at the indicated curent values. The injected current I is defined here as $I = qd \int C(x,y)dxdy$, where q is the electron charge and d the depth of the quantum well.

4.2 Gain Guided Devices

For gain guided devices, a frequency dependent complex susceptibility is taken into account through the complete set of equations (6)-(9) of the SFM model. For semiconductor lasers carrier dynamics produce an antiguiding effect, as explained in section 6. However, for VCSELs, this effect is overcome by thermally induced guiding associated with thermal lensing. This situation of overall guiding can be modeled within the two-level type susceptibility (13),(14) implied by (6)-(9) choosing a positive sign of α.

A typical example of the L-I characteristics that follow from the numerical integration of (6)-(9) for a circular contact VCSEL is shown in Figure 5 (Martín-Regalado et al., 1997a). These results correspond to a contact diameter of 10 μm and cavity anisotropy parameters $\gamma_p = 3.0\gamma_e$ and $\gamma_a = -5.0\gamma_e$. Given the frequency dependence of the gain and the positive detuning ($\alpha > 0$), the $\hat{y}$-polarized mode has a larger material gain and it would be selected at threshold for $\gamma_a = 0$. A cavity gain/loss anisotropy ($\gamma_a < 0$) has been introduced to overcome the material gain anisotropy induced by birefringence. In this way the total net gain for the $\hat{x}$–polarized mode is higher than that for the $\hat{y}$–polarized mode and $\hat{x}$-polarized emission is selected at threshold. The frequency splitting between the two polarization modes of the fundamental transverse mode is $\Delta\nu \sim$5.6 GHz, as calculated from Eqs.(22),(25). This situation corresponds then to the one considered in Figure 4 of selection of the $\hat{x}$–polarized mode at threshold and low birefringence ($\gamma_p < \gamma_s/2\alpha$).

Figure 5 shows that the VCSEL switches-on in the $\hat{x}$-polarized TEM_{00} mode, because of the effect of the cavity anisotropy. For increasing current, an $\hat{x} \rightarrow \hat{y}$ polarization switching is observed

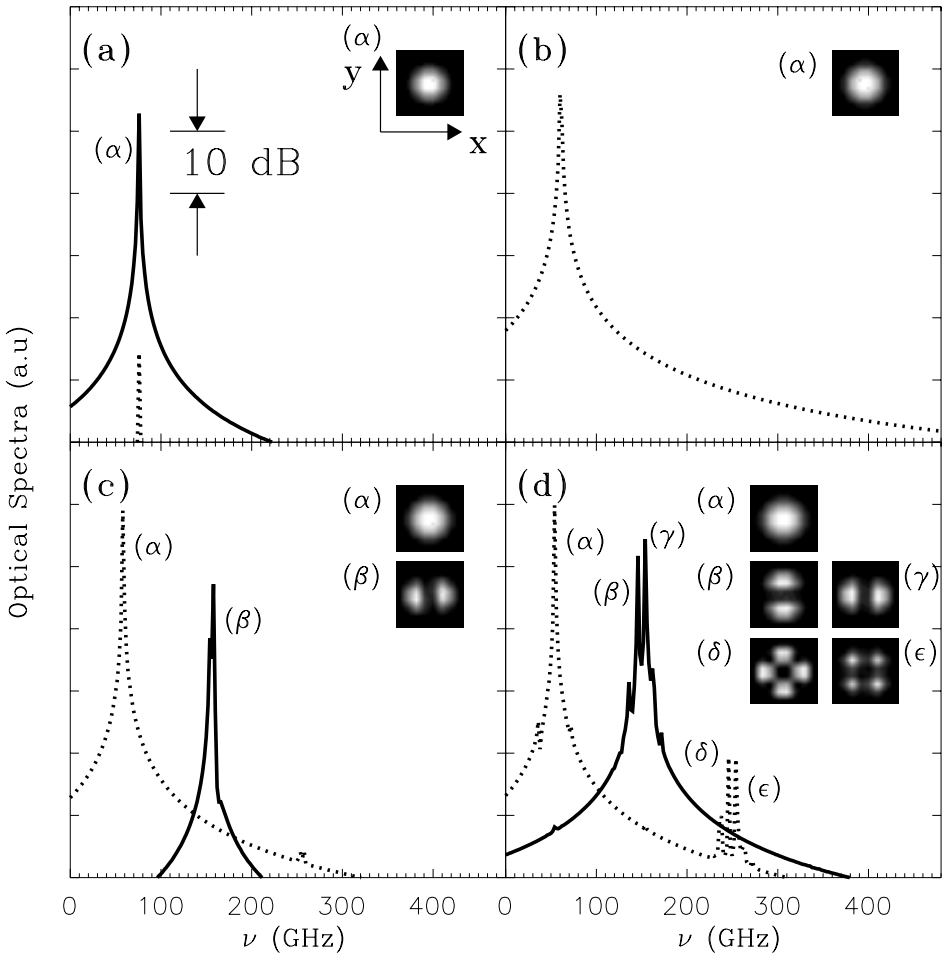

Figure 6: Optical spectra of the linearly polarized field components E_x (solid) and E_y (dashed) for the fixed current values indicated in Figure 5 by arrows: (a) $I = 1.29I_{th}$, (b) $I = 1.67I_{th}$, (c) $I = 1.87I_{th}$, (d) $I = 2.26I_{th}$.

at $I \sim 1.45I_{th}$, while the mode profile does not change. The switching current depends on the value of γ_a, (i.e. for $\gamma_a = -2.5\gamma_e$ switching occurs at $I \sim 1.30I_{th}$). For $I \sim 1.7I_{th}$ a first order transverse mode starts lasing. This mode is orthogonally polarized to the fundamental one. During the multitransverse mode regime ($I > 1.7I_{th}$), the $\hat{x}$-polarized total power increases almost linearly, while the $\hat{y}$-polarized total power saturates. For wider VCSELs with the same parameter values, the range of values of injection current in which the fundamental mode dominates is smaller. In some case switching is then not observed because of the early emergence of higher order transverse modes. The polarization and transverse mode competition obtained here reproduces the general phenomenology discussed in section 1.

The modal behavior of the VCSEL emission can be obtained by integrating (6)-(9) at a fixed current value instead of using a current ramp, as was done in Figure 5. Figure 6 shows the optical spectra and the transverse mode profiles obtained at four different injection current values. These spectra are equivalent to those obtained by a Fabry-Perot interferometer with a free spectral range of 1000 GHz and a frequency resolution of 2 GHz. At $I \sim 1.29I_{th}$, the polarized spectrum in Figure 6a shows that the laser mainly emits in the $\hat{x}$-TEM_{00} mode. However, the orthogonal polarization shows a strongly suppressed peak ($\sim$-40 dB). Beyond the switching current, at $I \sim 1.67I_{th}$, laser emission occurs in the $\hat{y}$-polarized Gaussian mode (Figure 6b). For increasing current, $I \sim 1.87I_{th}$, two transverse modes, the TEM_{00} (α) and the TEM_{10} (β), coexist, but with different polarizations

(Figure 6c).

Figure 6d shows the spectrum at $I \sim 2.26 I_{th}$. Several transverse modes are active in each polarization. It is remarkable that the two linear polarizations choose to operate in modes of different parity. Even order modes are $\hat{y}$-polarized (a dominant TEM_{00} mode (α), and some strongly suppressed second order modes (δ and ϵ)), while $\hat{x}$-polarized modes have odd order profiles (TEM_{10} (β) and TEM_{01} (γ) modes). Contrary to the cases shown in Figure 6a-c, where the total intensity emitted in each polarization is constant in time, the output of the laser oscillates in time for the injection current of Figure 6d. The total $\hat{x}$-polarized power is modulated at twice the beat note of the $\hat{x}$-polarized first-order transverse modes ($\approx 17\ GHz$). Periodic modulation at twice the beat frequency is also observed in the total $\hat{y}$-polarized power but, in this case, as a consequence of the nonlinear coupling between the two linearly polarized field components and the total carrier population.

It is interesting to consider the sensitivity of the dynamics just described to the value of the spin flip rate parameter γ_s to see the effect of the mixing of the carrier populations with different spin numbers. For a spin-flip relaxation rate ten times faster ($\gamma_s = 500\gamma_e$) than the one considered above, the dynamics turns out to be polarization independent. Polarization stability is observed in the fundamental mode regime. In addition, transverse modes start lasing with the same polarization that the fundamental mode and they appear at a much larger current $I \sim 2.25 I_{th}$. These features indicate that the selection of a particular transverse mode does not *only* depend on the modal gain when the spin-flip dynamics is not too fast and that physical mechanisms associated with the spin-flip relaxation rate are crucial in determining the transverse and polarization properties of gain-guided VCSELs.

5 Optically Pumped VCSELs

So far electrically pumped VCSELs have been implicitly considered. From the point of view of the scheme with two two-level systems of Figure 1b, this implies assuming that the two transitions are pumped with equal strength. Pumping the VCSEL optically with an off-resonance field allows to favor selectively one of the two lasing transitions by changing the ellipticity of the pump. When the pump is not linearly polarized, pumping creates a nonzero macroscopic magnetization $m_z \sim n$ by producing carriers with a preferred spin orientation. In this way the spin dynamics is unmasked and its effects become more apparent. Optically pumped VCSELS are thus very useful for fundamental studies of polarization selection mechanisms and other more general properties of VCSEL dynamics. Note also that the optical pump avoids, to a large extent, temperature effects (mostly due to selfheating) that complicate the interpretation of experimental results. From a more practical point of view, optical pumping can be useful to obtain self-sustained polarization oscillations, thanks to a more effective coupling of the two lasing transitions associated with right and left circularly polarized light.

For a VCSEL operating in the fundamental transverse mode the effect of optical pump is taken into account (Gahl et al., 1998) replacing Eqs.(17)-(18) by

$$\frac{dN}{dt} = -\gamma_e(N - (\eta_+ + \eta_-)) - \gamma_e(N+n)|E_+|^2 - \gamma_e(N-n)|E_-|^2 \tag{30}$$

$$\frac{dn}{dt} = \gamma_e(\eta_+ - \eta_-) - \gamma_s n - \gamma_e(N+n)|E_+|^2 + \gamma_e(N-n)|E_-|^2 \tag{31}$$

where η_+ (η_-) is the optical pump of the $E_+(E_-)$ field component, so that the pump ellipticity is given by $P = (\eta_+ - \eta_-)/(\eta_+ + \eta_-)$. Information on the carrier and spin dynamics is then obtained by studying the ellipticity of the output laser light as a function of P. An additional way of probing spin dynamics is introducing a magnetic field B_x in the direction transverse to that of light emission (Voigt geometry). The magnetization associated with n is then subject to Larmor precession, which

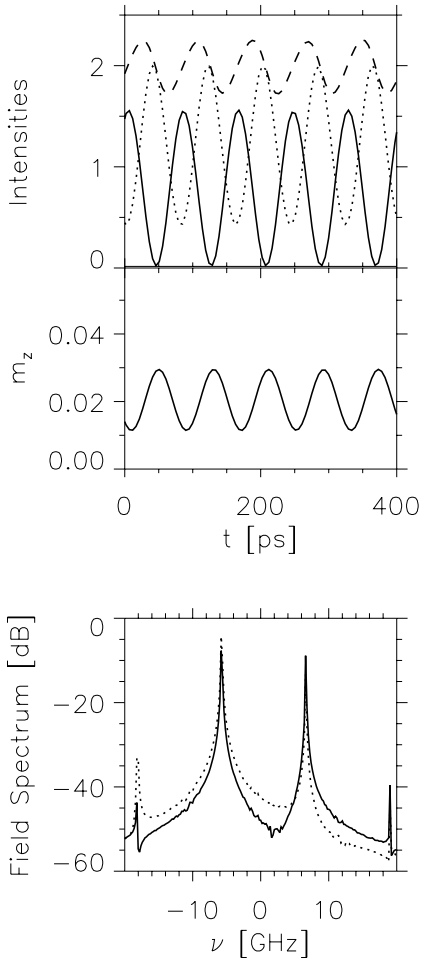

Figure 7: Time series of the polarization resolved intensities (full curve: $I_+ = |E_+|^2$, dotted curve: $I_- = |E_-|^2$), the total intensity $I_+ + I_-$ (dashed curve), the magnetization component $m_z = n$ and the corresponding field spectra (full curve: E_+, dotted curve: E_-); parameters: $\eta = \eta_+ + \eta_- = 3$, $P = 0.9$, $\gamma_e = 1\text{ns}^{-1}$, $\kappa/\gamma_e = 250$, $\gamma_p/\pi = 12\text{GHz}$, $\gamma_a/\gamma_p = 0.01$, $\alpha = 3$, $\gamma_s/\gamma = 150$.

yields another coupling of the two spin sublevels of the conduction band. The theoretical description of this situation requires the consideration of an additional coupled variable which represent the magnetization along the transverse direction perpendicular to the magnetic field. This variable also represents the quantum coherence between the two electron spin sublevels of Figure 1b, under the assumption of very fast hole spin relaxation.

From a fundamental point of view, consideration of an optically pumped VCSEL in a transverse magnetic field can be used to determine the spin flip rate γ_s by measuring the laser light ellipticity as a function of magnetic field strength for a circularly polarized pump, $P = 1$ (Hanle effect). It follows from the model considered here that the ellipticity, normalized to the zero magnetic field ellipticity, is a Lorentzian whose width scales as B_x/γ_s, with no other adjustable parameters (Gahl et al., 1998). This model also gives a good description of light oscillations at the Larmor frequency which have been observed in a VCSEL pumped with a pulse of 2 psec of elliptically polarized light in a transverse magnetic field of 2 Tesla (Hallstein et al., 1997). Such studies, in which the nonlinear regime above the laser threshold is considered, parallel fundamental studies of spin relaxation properties in semiconductor materials with no optical cavity (Kikkawa et al., 1997; Kikkawa and Awschalom, 1998). In the latter stuides one is in fact considering a linear regime below a laser threshold.

It is rather natural to expect polarization oscillations if the SFM model is considered from a dynamical systems point of view. Each of the two two-level systems in Figure 1b is a nonlinear oscillator and they are coupled through carrier dynamics (spin flip and eventually a transverse magnetic field) and through the optical fields by birefringence. The coupled system has several natural frequencies (relaxation oscillations, birefrigence frequency splitting, Larmor oscillations in magnetic field) of comparable magnitude (from a few to tens of GHz). Nonlinear coupling among the two subsystems can produce the unstabilization of any of these oscillations by means of harmonic or beat note excitation, thus leading to self-sustained oscillations in the polarization of the emitted light under continuous pump. As an example, Figure 7 shows self-sustained polarization oscillations at a frequency dictated by birefringence as obtained from the numerical integration of Eqs.(16),(30),(31) for a pump with an ellipticity close to being circularly polarized. The oscillations occur for a value of the birefringence which is comparable with the difference between the natural frequencies of the two lasing transitions which is created by the α-factor when the laser operates at $n \neq 0$. Oscillations disappear for birefringences much larger or smaller than this value.

Polarization oscillations and other dynamical states can also occur, as previously mentioned, under electrical pump. However, optical pump is much more versatile and permits to obtain these states under a much broader range of situations and for easily attainable values of the physical parameters of the VCSEL.

6 Beyond a two-level susceptibility

The discussion in sections 3-5 considers a model based on a two-level type susceptibility (12)-(14), where α appears as a detuning. This model has allowed to obtain a good number of results within a relatively easy description. However, there are important differences between a two-level type susceptbility χ and the typical one of a semiconductor quantum well laser. Such differences modify the frequency dependent dynamics when several transverse modes come into play, and also in the case of operation in the fundamental transverse mode. The origin of these differences is that a semiconductor can be regarded as a collection of two-level transitions, each one for each transverse wavenumber in the semiconductor band structure. Summation over these transverse wavenumbers leads to the differences shown schematically in Figure 8, where gain$\sim -Im\chi$ and index $\sim Re\chi$.

One important difference is the relation between the detuning and the guiding effects of the carriers. In the two level susceptibility the gain curve is symmetric and the frequency of maximum gain does not change with carrier injection. The nonlinear contribution to the index of refraction vanishes at the frequency of maximum gain and the change of index of refraction with carrier number depends on the sign of the detuning: For a positive detuning ($\Delta > 0$) the index increases with carrier number (carrier guiding) while for negative detuning it decreases (carrier antiguiding). On the contrary, in a semiconductor the gain curve is not symmetric and the frequency of maximum gain shifts with carrier number. Grossly speaking, the index grows monotonically with frequency in the frequency range of positive gain. In this range the index decreases with increasing carrier number for any sign of the detuning. Such antiguiding effect corresponds to a negative value of the parameter α as defined in (15). The consequence is that the intrinsic anitiguiding effect of a semiconductor is independent of detuning, while within a two level model guiding or antiguiding are dictated by detuning.

In section 4 it was argued that there is an overall guiding effect in the VCSEL due to thermal lensing. This was taken into account choosing a positive detuning ($\alpha > 0$). In addition, in the derivation of Eqs.(16)-(18), which have been used to describe operation in the fundamental transverse mode, the frequency dependence of gain and index was eliminated. To overcome the shortcomings of this description there are two main alternatives. A first one is to introduce a full many body

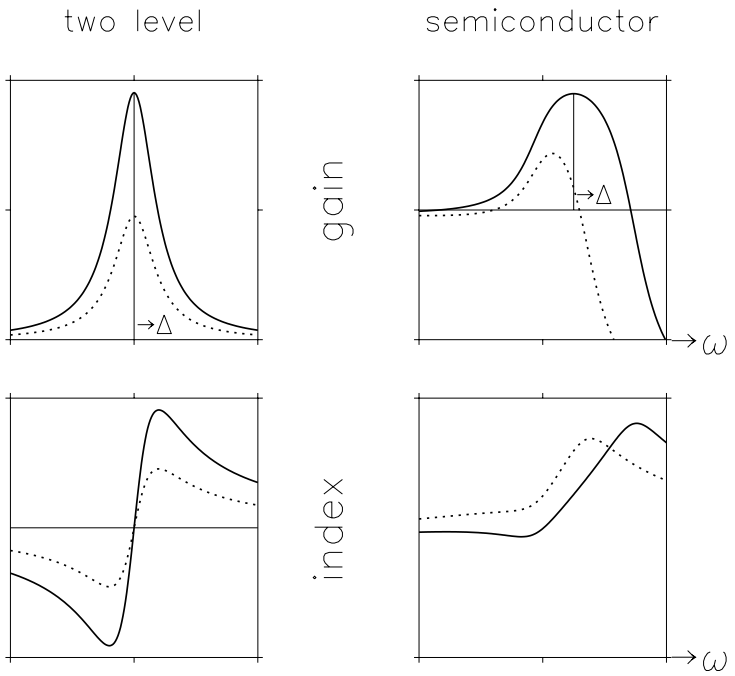

Figure 8: Schematic plot of the frequency dependence of the complex susceptibility for a two level model and a semiconductor. Dashed and continuous lines correspond to two different values of the carrier number density (pumping level), being the carrier density number smaller for the dashed line. The vertical line indicates the frequency of maximum gain and Δ indicates detuning with respect to this frequency.

description of the semiconductor dynamics (Chow et al., 1994). This gives a correct fundamental description in which different effects are incorporated, but at the cost of high conceptual and computational complexity. For a broad range of situations a second viable and practical alternative is to extract from those microscopic theories the effects that have important consequences and to introduce them, through an approximated susceptibility, in a macroscopic description which still has the conceptual simplicity of a two-level system. An example of this type of approach is based on an approximated calculation of the susceptibility of a quantum well (Balle, 1998). This is a low temperature and quasiequilibrium calculation which only considers the conduction and heavy-hole bands within a parabolic approximation. It also assumes charge neutrality and the summation over transverse wavenumbers is over the first Brillouin zone. The result can be written, for each of the two transitions associated with the two circularly polarized components of light, as

$$\chi_{\pm}\left(\omega_{\pm}, D_{\pm}\right) = -\chi_0 \left[ln\left(1 - \frac{2D_{\pm}}{u_{\pm} + i}\right) + ln\left(1 - \frac{D_{+} + D_{-}}{u_{\pm} + i}\right) - ln\left(1 - \frac{b}{u_{\pm} + i}\right)\right] \tag{32}$$

where

$$u_{\pm} = \frac{\omega_{\pm}}{\gamma_{\perp}} + \Delta + \sigma(D_{+} + D_{-})^{1/3}, \qquad \Delta = \frac{\nu - \omega_g}{\gamma_{\perp}} \tag{33}$$

and b gives the background refraction index. $D_{\pm}$ have the same meaning as discussed after Eq.(9), $\omega_{\pm}$ are the frequencies of the two transitions and the detuning Δ formally coincides with α in (10). Band-gap renormalization effects have been additionally included in this expression for the susceptibility through the term proportional to σ in the definition of $u_{\pm}$. This term describes the known functional dependence of band-gap shrinkage with carrier number and σ is a free parameter of the model. This form of the susceptibility accounts very well for the general features described in connection with Figure 8. The definition (15) gives now a frequency dependent α-factor. Its value at the frequency of maximum gain has the correct known dependence with carrier number (Balle, 1998).

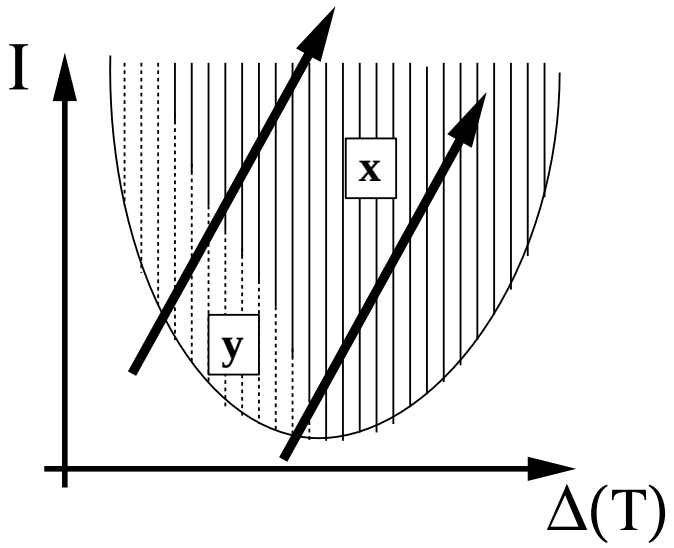

Figure 9: Approximated parabolic dependence of the threshold current as a function of the detuning Δ as predicted by (35)-(35). Δ is a function of temperature T. Vertical lines indicate the polarization state selected as the injection current I is raised at constant detuning. Dashed (solid) lines correspond to a $\hat{y}$ ($\hat{x}$)linearly polarized state. The arrows indicate two possible paths for polarization switchings as explained in the text.

An additional important point of (32) is that a main thermal effect can be easily taken into account by letting the detuning parameter Δ to depend on temperature. Indeed, it was mentioned in section 1 that heating of the device changes the relative position of the resonant cavity frequency and the frequency of maximum gain. This can be described by changing Δ as temperature or injection current rise.

The SFM model can now be written using the susceptibility (32) and the relation (12) in (3), together with Eqs.(8)-(9) for the carriers. For operation in the fundamental transverse mode, so that diffraction and carrier diffusion are neglected, the equations for the fields $F_\pm$ and carrier populations $D_\pm$ of the two transitions in Figure 1b can be written as,

$$\dot{F}_\pm = -\kappa F_\pm + ia\chi_\pm(\omega_\pm, D_\pm) F_\pm - (\gamma_a + i\gamma_p) F_\mp \tag{34}$$

$$\dot{D}_\pm = I - \gamma_e D_\pm - \gamma_j (D_\pm - D_\mp) + \frac{2\epsilon_0}{\hbar} Im[\chi_\pm(\omega_\pm, D_\pm)] |F_\pm|^2 \tag{35}$$

where I is the injected current. A proper description of frequency dependent dynamics is obtained solving (35)-(35) imposing selfconsistently that $\omega_\pm = -i\dot{E}_\pm/E_\pm$.

A schematic summary of the results that follow from this model and negligeable values of γ_a is given in Figure 9. There is a minimum threshold current for a detuning value $\Delta = \Delta_m$. The selected state at threshold is the one that has larger material gain, which is different for $\Delta > \Delta_m$ and for $\Delta < \Delta_m$ due to the frequency splitting of the two polarization modes caused by birefringence. If polarization selection were just a question of relative gain the selected state would be the same for all values of injected current and a fixed value of Δ. A temperature induced switching (Choquette et al., 1995b) would occur because the sign of $\Delta - \Delta_m$ changes as the pump increases. However, what is predicted is that for a fixed value of Δ there is a switching for a particular value of the injection current if $\Delta < \Delta_m$, while no switching occurs for $\Delta > \Delta_m$. This situation corresponds to the analysis of Figures 3 and 4 for $\gamma_p > \gamma_s/(2\alpha)$. The preference for a particular polarization at threshold was obtained in Figures 3 and 4 by the sign of γ_a. Here it is a consequence of the frequency dependence of the gain curve.

The physical mechanisms of polarization switching at constant Δ in Figure 9 are the ones pre-

viously discussed and associated with phase-amplitude coupling and spin dynamics. However, in reality polarization switching does not occur at constant Δ unless the laser is pumped with electrical pulses shorter than the thermal relaxation time. In general, increasing the injection current leads to a temperature rise, and Δ increases with temperature, so that the path followed in the parameter space I, Δ is the one indicated by the arrows in Figure 9. Polarization switching occurs when the border line between the two domains of polarization selection, indicated by solid and dashed lines, is crossed. In the generic situation of the upper arrow switching occurs for a detuning $\Delta < \Delta_m$ and it leads from the mode of higher linear gain to the one of lower linear gain for that value of Δ. For the special case of the lower arrow, polarization switching happens to occur at Δ_m, as it is predicted for a polarization switching which were just the result of a thermal effect.

Acknowledgments

I wish to thank the colleagues and collaborators that have contributed in different research papers to ideas and results discussed in these lectures: N. B. Abraham, S. Balle, Q. Feng, A. Gahl, J. Martin-Regalado, J. Moloney, L. Pesquera, F. Prati, C. Serrat, A. Valle and R. Vilaseca. Work partially supported by the European Union under Project FMRX-CT96-066.

References

Agrawal, G. P. and Dutta, N. K. (1986). *Longwavelength Semiconductor Lasers*. Van Nostrand, New York.

Balle, S. (1998). *Phys. Rev. A*, 57:1304.

Bar-Ad, S. and Bar-Joseph, I. (1992). *Phys. Rev. Lett.*, 68:349.

Blum, O. (1999). Materials issues. In Miller, A., editor, *Semiconductor Quantum Optoelectronics*. Institute of Physics.

Britton, R. S., Grevatt, T., Malinowski, A., Harley, R., Perozzo, P., Cameron, A. R., and Miller, A. (1998). *Appl. Phys. Lett.*

Chang-Hasnain, C. J., Harbison, J. P., Hasnain, G., VonLehmen, A. C., Florez, L. T., and Stoffel, N. G. (1991). *IEEE J. Quantum Electron.*, 27:1402.

Chavez-Pirson, A., Ando, H., Saito, H., and Kanbe, H. (1993). *Appl. Phys. Lett.*, 62:3082.

Choquette, K. D., Lear, K. L., Leibenguth, R. E., and Asom, M. T. (1994a). *Appl. Phys. Lett.*, 64:2767.

Choquette, K. D., Lear, K. L., Schneider, R. P., Leibenguth, R. E., Figiel, J., Kilcoyne, S. P., Hagerott-Crawford, M., and Zolper, J. C. (1995a). In *Laser Diodes and Applications, Vol. 2382*, page 125. SPIE.

Choquette, K. D., Richie, D. A., and Leibenguth, R. E. (1994b). *Appl. Phys. Lett.*, 64:2062.

Choquette, K. D., Schneider, R. P., Lear, K. L., and Leibenguth, R. E. (1995b). *IEEE J. Select. Topics Quantum Electron.*, 1:661.

Chow, W. W., Koch, S. W., and Sargent, M. (1994). *Semiconductor Laser Physics*. Springer-Verlag, Berlin.

Damen, T. C., Vina, L., Cunningham, J. E., Shah, J., and Sham, L. J. (1991). *Phys. Rev. Lett.*, 67:3432.

de Lang, H., Polder, D., and VanHaeringen, W. (1971). *Phillips Tech. Rev.*, 32:190.

Ebeling, K. J. (1999). Vertical Cavity Surface Emitting Lasers. In Miller, A., editor, *Semiconductor Quantum Optoelectronics*. Institute of Physics.

Epler, J. E., Gehsitz, G., Gulden, K. H., Moser, M., Sigg, H. C., and Lehmann, H. W. (1996). *Appl. Phys. Lett.*, 69:722.

Fiedler, U., Reiner, G., Schnitzer, P., and Ebeling, K. J. (1996). *IEEE Photon. Technol. Lett.*, 8:746.

Fishman, G. and Lampel, G. (1977). *Phys. Rev. B.*, 16:820.

Gahl, A., Balle, S., and SanMiguel, M. (1998). *Quantum and Semiclass. Opt.*, 10:L1.

Hallstein, S., Berger, J. D., Hilpert, M., Schneider, H. C., Ruhle, W. W., Jahnke, F., Koch, S. W., Gibbs, H. M., Khitrova, G., and Ostreich, M. (1997). *Phys. Rev. B*, 56:R7076.

Hendriks, R. F. M., van Exter, M. P., Woerdman, J. P., van Geelen, A., Weegels, L., Gulden, K. H., and Moser, M. (1997). *Appl. Phys. Lett.*, 71:2599.

Henry, C. H. (1982). *IEEE J. Quant. Electron.*, 18:259.

Kawaguchi, H., Hidayat, I. S., Takahashi, Y., and Yamayoshi, Y. (1995). *Electron. Lett.*, 31:109.

Kawaguchi, H. and Kawakami, T. (1977). *IEEE J. Selected Topics in Quantum Electron.*, 3:1254.

Kikkawa, J. M. and Awschalom, D. D. (1998). *Phys. Rev. Lett.*, 80:4313.

Kikkawa, J. M., Smorchkowa, I. P., Samarth, N., and Awschalom, D. D. (1997). *Science*, 277:1284.

Koyama, F., Morito, K., and Iga, K. (1991). *IEEE J. Quantum Electron.*, 27:1410.

Lenstra, D. (1980). *Phys. Reports*, 59:299.

Li, H., Lucas, T. L., McInerney, J. G., and Morgan, R. A. (1994). *Chaos, Solitons and Fractals*, 4:1619.

Martin-Regalado, J. (1997). *Polarization Properties of Vertical Cavity Surface Emitting Lasers (http://www.imedea.uib.es/PhysDept/publicationsDB)* . PhD thesis, Universitat Illes Balears, Palma de Mallorca, Spain.

Martín-Regalado, J., Balle, S., and SanMiguel, M. (1997a). *Opt. Lett.*, 22:460.

Martín-Regalado, J., Balle, S., SanMiguel, M., Valle, A., and Pesquera, L. (1997b). *Quantum and Semiclass. Opt.*, 9:713.

Martín-Regalado, J., Chilla, J. L. A., Rocca, J. J., and Brusenbach, P. (1997c). *Appl. Phys. Lett.*, 70:3350.

Martín-Regalado, J., SanMiguel, M., Abraham, N., and Prati, F. (1997d). *IEEE J. Quantum Electron.*, 33:765.

Meier, F. and Zachachrenya, B. P., editors (1984). *Optical orientation*. North Holland, Amsterdam.

Miller, A. (1999). In Miller, A., editor, *Semiconductor Quantum Optoelectronics*. Institute of Physics.

Mukaihara, T., Koyama, F., and Iga, K. (1993). *IEEE Phot. Tech. Lett.*, 5:133.

Nishikawa, Y., Tackeuchi, A., Nakamura, S., Muto, S., and Yokoyama, N. (1995). *Appl. Phys. Lett.*, 66:839.

Oestreich, M., Hallstein, S., and Rühle, W. W. (1996). *IEEE J. Selected Topics in Quant. Electron.*, 2:747.

Osinski, M. and Buus, J. (1987). *IEEE J. Quant. Electron.*, 23:9.

Pan, Z., Jiang, S., Dagenais, M., Morgan, R., Kojima, K., Asom, M., Leibenguth, R., Guth, G., and Focht, M. (1993). *Appl. Phys. Lett.*, 63:2999.

Panajotov, K., Ryvkin, B., Danckaert, J., Peeters, M., Thienpont, H., and Veretennicoff, I. (1998). *IEEE Photon. Technol. Lett.*, 10(1):6.

SanMiguel, M., Feng, Q., and Moloney, J. V. (1995). *Phys. Rev. A*, 52:1728.

Sargent, M., Scully, M. O., and Lamb, W. (1974). *Laser Physics.* Addison Wesley, New York.

Ser, J. H., Ju, Y. G., Shin, J. H., and Lee, Y. H. (1995). *Appl. Phys. Lett.*, 66:2769.

Serrat, C., Abraham, N. B., SanMiguel, M., Vilaseca, R., and Martín-Regalado, J. (1996). *Phys. Rev. A (Rapid Comm.)*, 53:R3731.

Sham, L. J. (1993). *J. Phys. Condens. Matter*, 5:A51.

Snelling, M., Flinn, G., Plau, A., Harly, R., and Tropper, A. (1991). *Phys. Rev. B*, 44:11345.

Stephan, G. M. and May, A. D. (1998). *Quantum and Semiclass. Opt.*, 10:19.

Sun, D., Towe, E., Otsdiek, P. H., Grantham, J. W., and Vansuch, G. J. (1975). *IEEE J. Selected Topics in Quantum Electron.*, 1:674.

Tackeuchi, A., Nishikawa, Y., and Wada, O. (1996). *Appl. Phys. Lett.*, 68:797.

Valle, A., Martin-Regalado, J., Pesquera, L., Balle, S., and SanMiguel, M. (1998). In *Physics and Simulation of Optoelectronic Devices VI.* SPIE.

Valle, A., Sarma, J., and Shore, K. A. (1995). *IEEE J. Quantum Electron.*, 31:1423.

Valle, A., Shore, K. A., and Pesquera, L. (1996). *IEEE J. of Lightwave Tech.*, 14:2062.

van der Lem, H. and Lenstra, D. (1997). *Optics Lett.*, 22:1698.

van der Lem, H., Martín-Regalado, J., Balle, S., and Mirasso, C. (1998). *IEEE Photon. Tech. Lett.*, 10:21.

van Doorn, A. J., van Exter, M., and Woerdman, J. (1996a). *Appl. Phys. Lett.*, 69:3635.

van Doorn, A. K. J., van Exter, M. P., and Woerdman, J. P. (1996b). *Appl. Phys. Lett.*, 69:1041.

van Doorn, A. K. J., van Exter, M. P., Woerdman, J. P., and Travagnin, M. (1997). *Opt. Commun.*, 133:252.

van Exter, M. P., Al-Remawi, A., and Woerdman, J. P. (1998a). *Phys. Rev. Lett.*, 80:4875.

van Exter, M. P., Hendriks, R. F. M., and Woerdman, J. P. (1998b). *Phys. Rev. A*, 57:2080.

van Haeringen, W. (1967). *Phys. Rev.*, 158:256.